THE JOURNAL OF PHYSICAL CHEMISTRY B

Article

pubs.acs.org/JPCB

# Evaporation of Tiny Water Aggregation on Solid Surfaces with Different Wetting Properties

Shen Wang,[†,‡] Yusong Tu,[§] Rongzheng Wan,*[,†] and Haiping Fang[†]

[†]Shanghai Institute of Applied Physics, Chinese Academy of Sciences, P.O. Box 800-204, Shanghai, 201800, China

[‡]Graduate School of the Chinese Academy of Sciences, Beijing 100080, China

[§]Institute of Systems Biology, Shanghai University, Shanghai, 200444, China

Supporting Information

**ABSTRACT:** The evaporation of a tiny amount of water on the solid surface with different wettabilities has been studied by molecular dynamics simulations. From nonequilibrium MD simulations, we found that, as the surface changed from hydrophobic to hydrophilic, the evaporation speed did not show a monotonic decrease as intuitively expected, but increased first, and then decreased after it reached a maximum value. The analysis of the simulation trajectory and calculation of the surface water interaction illustrate that the competition between the number of water molecules on the water−gas surface from where the water molecules can evaporate and the potential barrier to prevent those water molecules from evaporating results in the unexpected behavior of the evaporation. This finding is helpful in understanding the evaporation on biological surfaces, designing artificial surfaces of ultrafast water evaporating, or preserving water in soil.

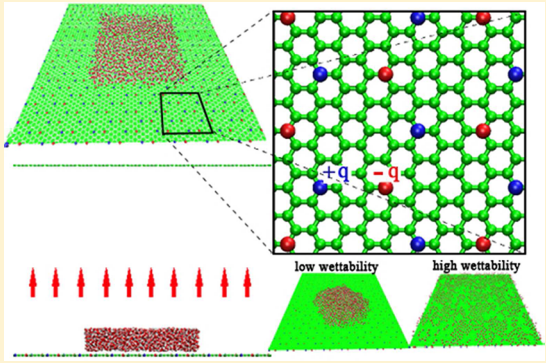


## INTRODUCTION

The evaporation of water is very important in biological[1] and environmental[2] science. The water evaporation of a bulk surface, such as a lake or a river, is a classical topic and has been studied for a long time.[2−4] Recent works show that the nanoscale confined water and water restricted on the surface of solid materials are ubiquitous in nature,[5−15] for example, the icelike water monolayer on top of a hydrophilic[6,16,17] or a hydrophobic[18−23] solid surface. The evaporation of such a nanoscale water aggregation is essential in the macroscopic world, for example, the water loss through the surface of soil,[24] and gas−liquid phase transition of water aggregation above the surfactant,[25−27] and the evaporation of the surficial water aggregation also plays an important role in biophysical phenomena, such as the folding of globular protein.[28−31] The evaporation of such a confined water aggregation is different from the classical evaporation of bulk water. Very recently, Lee and his co-workers have used a scanning electron microscope to study the evaporation efficiency of microscaled water droplets from nanoporous microcantilevers of various hydrophobicities and stated that the dynamics of water evaporation between hydrophobic and hydrophilic conditions are very different.[32,33] However, how the surface wettability affects the evaporation of the tiny water aggregation still remains unclear.

Here, we present molecular dynamics (MD) simulations[34−36] on the evaporation of a nanoscale water aggregation on a solid substrate with different surface wettabilities at room temperature. The water aggregation was adhered to a solid wall-like substrate, and the thickness of the water layer was less than 1 nm. The simulations showed that the evaporation speed of the water aggregation first increased as the surface wettability increased when the surface wettability was not high enough; then the evaporation speed decreased as the surface wettability was further increased. We found that the surface wettability could affect the evaporation flux in two mechanisms: the increasing of surface wettability enhances the evaporation flux by increasing the area of the liquid−gas surface of the water aggregation, and increasing the surface wettability reduces the evaporation flux by increasing the escape energy barrier of surficial water molecules. The final evaporation speed of nanoscale water aggregation is the competition of these two mechanisms. When the surface wettability is low, the surface wettability dominatingly increases the area of the liquid−gas surface, which causes the increase of the evaporation speed; after the surface wettability becomes high enough, the surface wettability dominatingly increases the escaping energy barrier of surficial water molecules, which causes the evaporation speed to decrease.

## SIMULATION METHOD

MD simulations were carried out in a box with an initial size of 13.5 nm × 11.8 nm × 11.0 nm. The periodic boundary condition was applied to all three independent Cartesian coordinates $x$, $y$, and $z$. Similar to the work of Wang et al,[37] the

**Received:** March 5, 2012
**Revised:** October 10, 2012
**Published:** October 11, 2012

   dx.doi.org/10.1021/jp302142s | J. Phys. Chem. B 2012, 116, 13863−13867

substrate had dimensions of 13.5 nm × 11.8 nm with a planar hexagonal structure of neighboring bond lengths of 0.142 nm. As shown in Figure 1a,b, positive and negative charges of the same magnitude $q$ were assigned on the atoms at a distance of 0.568 nm (2 times the diagonal of the hexagon). Overall, the substrate contained 192 positive charges and 192 negative charges and was neutral. By changing $q$, we obtained a solid surface with a tunable wettability that was inspired by the laboratory available polar surface.[38−41]This graphene-like sheet lay on the bottom of the cell along the $x$−$y$ plane as a substrate, above which the water monolayer was laid (Figure 1a,c). There was a total of 1298 water molecules in the system. The number of water molecules was slightly less than a monolayer of water with the assumption that one water monolayer on a flat surface is $1 \times 10^{15}$ molecules/cm$^2$.[42] An accelerating region was applied from 3 to 5 nm above the substrate, as shown in Figure 1c. When a water molecule ran into the accelerating region, a vertically upward force as strong as 1 kcal × mol$^{-1}$ A$^{-1}$ (force vector (0 0 1)) was applied on the oxygen atom of that water molecule to prevent the water molecule from going back to the substrate. Such a nonequilibrium condition is equivalent to the setting of some other literature that the evaporated molecules will run into an infinite vacuum or reach a zero potential point (infinitely far from the liquid).[43] There was a ceiling solid wall made by the same graphene-like sheet without assigned charges lying 10 nm higher to prevent the water molecules from reaching the bottom side of the substrate.

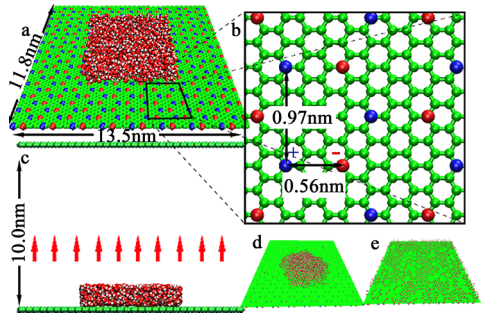


**Figure 1.** (a) The initial system. (b) Detailed geometry of the solid substrate model. Red and blue spheres represent the atoms with positive and negative charges, respectively, while the green spheres represent neutral atoms. (b) Side view of the initial system. The upward arrow denoted the accelerating region. (d) Snapshot of water on the substrate with low wettability; $q$ = 0 e. (e) Snapshot of water on the substrate with high wettability; $q$ = 0.7 e.

We used the Charmm22 force field with a rigid TIP3P[44] water model. The atoms in the graphene-like model solid substrate and the ceiling solid wall had the Lennard-Jones parameters $\varepsilon$ = 0.07 kcal/mol and $\sigma$ = 0.4 nm, which were borrowed from the aromatic carbon[45,46] and were frequently used for the study of carbon atoms in carbon nanotubes or graphene with NAMD. All the MD simulations were carried out by NAMD2.6[47] with a time step of 2 fs, and the particle mesh Ewald (PME) integration was employed with a frequency of once per four steps. The PME Grid sizes in $X$, $Y$, and $Z$ directions were $^1/_{128}$, $^1/_{128}$, and $^1/_{100}$ of the box size. All the water molecules were attached to a thermostat of 300 K, and a simple method of Berendsen temperature coupling[48] was applied every 20 steps, which was also the same frequency of atom reassignment. The trajectories of the coordinate and velocity were collected every 500 steps, that is, every 1 ps, and a total of 10 000 frames of datum were included in the trajectory files.

Initially, the 1298 water molecules were piled upon the substrate in a water cube of 6 nm × 6 nm × 1.2 nm, as shown in Figure 1a. The simulations were carried out following a two-stage protocol. Stage 1: A 10 ns equilibrium simulation (without the accelerating region) was carried out to relax the initial water cube to the equilibrium state. The water molecules formed a spherical-shaped sessile droplet on the substrate with low wettability (Figure 1d) or a smoothly spread monolayer on the substrate with high wettability (Figure 1e), and the wettability of the substrate can be evaluated by the contact angle of the water aggregation. Stage 2: A nonequilibrium MD simulation (with the accelerating region) was carried out to study the evaporation behavior of the water molecule.

## RESULT AND DISCUSSION

**Wettability of the Solid Surface.** We measured the wettability of the surface according to the trajectory of the 10 ns equilibrium molecular dynamics simulations. Figure 2a shows the probability density distribution of the water molecules along the normal direction of the solid surfaces with different charges $q$. The probability densities for $q \geq 0.4$ e are shown in an embedded graph in stacking frames since they are similar with each other. From Figure 2a, we find that, when $q < 0.4$ e, the density profile has two peaks, which indicates that, besides

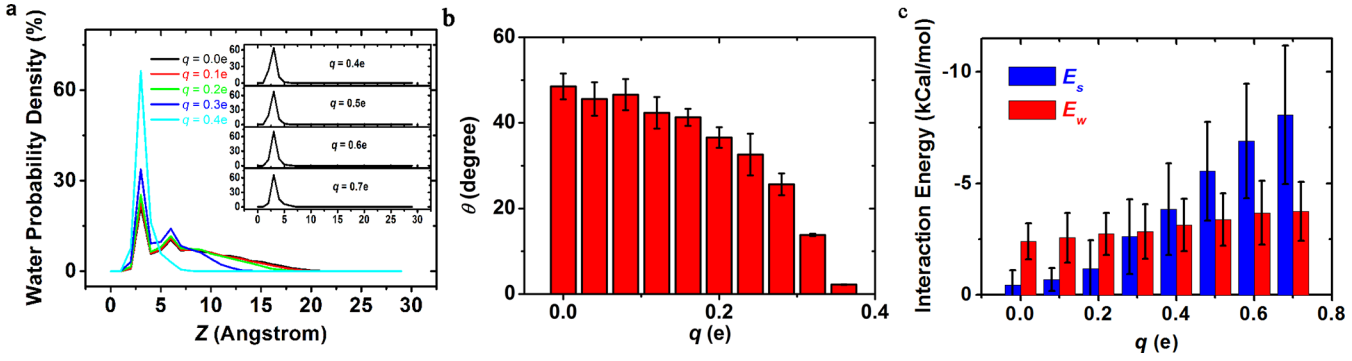


**Figure 2.** (a) The probability density distribution of the water oxygen atom along the normal direction to the solid surface. For $q$ = 0.0−0.4 e, the density profiles are draw together in different color lines, and the profiles for $q$ = 0.4−0.7 e are shown in the embedded serial stacked lines. (b) The contact angle of the water aggregation versus the assigned charge $q$ ($q$ = 0−0.4 e). (c) The interaction energy on the first hydration layer exerted by the solid surface (blue columns) and the pairwise water−water interaction (red columns).


dx.doi.org/10.1021/jp302142s | J. Phys. Chem. B 2012, 116, 13863−13867

the first hydration layer adjacent to the solid surface, there is at least another layer of water molecules. When $q \geq 0.4$ e, the probability density distributions are almost the same in shape with only one peak. The distance between the first hydration layer and the solid surface remains at 3 Å regardless of the variation of the surface charges.

The contact angle of the water droplet on a solid surface is a frequently used criterion in defining the wettability of a surface. We measured the contact angles $\theta$ of the water aggregation on different surfaces and have shown them in Figure 2b. From 0 e to 0.4 e, $q$ is sampled with an increment of 0.04 e so that the variation the contact angle can be sampled in more detail. For all the surfaces with $q \geq 0.4$ e, there is roughly one layer of water molecules and the contact angle can be defined as zero. The contact angle $\theta$ decreases as $q$ increases for $q < 0.4$ e, indicating a monotonic enhancing of the wettability of the surface. It is necessary to state that the contact angle of the water aggregation can also be affected by the amount of aqueous[49−51] or nearby liquid molecules[52] so that the contact angle $\theta$ measured in this work is involved only for the relative comparison of the wettability of the substrate and theoretically analysis of the result.

The wettability of the surface can also be described by $E_s$, which is the average interaction energy between the solid surface and the water molecules in the first hydration layer (within 3 Å of the solid surface). Figure 2c shows the competition between the average water−surface interaction energy $E_s$ (blue columns) and the pairwise water−water interaction energy $E_w$ (red columns) on the first hydration layer. When the surface charge $q$ increases, the water−surface interaction energy increases steadily; at $q$ = 0.4 e, $E_s$ first exceeds $E_w$. This explains the phenomenon in Figure 1d,e: when $q$ > 0.4e, $E_s$ wins over $E_w$, and the water molecules begin to spread across the surface.

**Evaporation Flux $J(q)$.** The evaporation speed of the water layer can be described by the evaporation flux $J(q)$, which is defined as the average number of water molecules entering the accelerating region from the substrate per nanosecond in unit area, since such water molecules will go upward until they reach the ceiling and will not go back to the substrate as condensed molecules. Counter to what is intuitively expected, the evaporation flux does not decrease monotonically with the enhancing of $q$. Actually, as shown in Figure 3a, the evaporation flux first increases from $0.95 \times 10^{-2}$ ns$^{-1}$ nm$^{-2}$ to its maximum value of $2.35 \times 10^{-2}$ ns$^{-1}$ nm$^{-2}$ around $q$ = 0.4 e. When $q \geq 0.4$ e, the evaporation flux decreases with the enhancing of $q$, and the evaporation flux $J(q)$ is only $1.07 \times 10^{-2}$ ns$^{-1}$ nm$^{-2}$ at $q$ = 0.7 e.

In Figure 3b, we show the accumulative number of the evaporated water molecules with respect to the time. Since the slope of each line almost remains constant, the evaporation speeds of the surficial water are stable. Such an evaporation characteristic is comparable to previous hydrodynamics[53] or molecular dynamics[54−57] studies and is very similar with the stationary nonequilibrium state of evaporation achieved by the "open lid" method employed by Zhakhovskii.[40] The constant evaporation speeds suggested that the current setting of the simulation system is valid for the comparison of the evaporation speeds of surficial water upon asolid surface with different wettabilities.

We assume that the evaporation flux $J(q)$ can be denoted as a product of the probability for a water molecule to be on the liquid−gas surface of the water molecule aggregation and the escape probability of such a surficial water molecule.

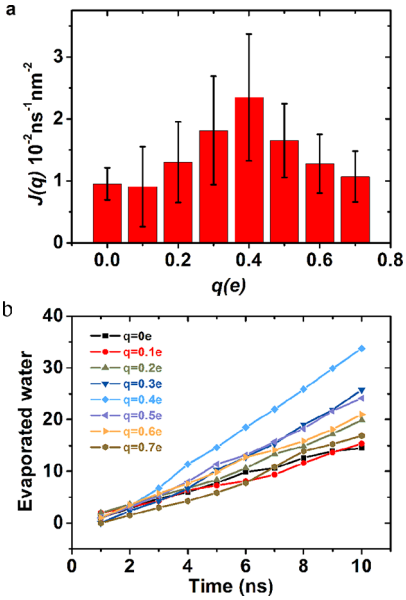


**Figure 3.** (a) Evaporation flux and its error versus different assigned charges $q$. (b) The accumulative number of evaporated water molecules during the simulation versus time.

$$J(q) \propto P_{geo}(\theta(q))P_{ener}(E) \quad (1)$$

Here, $P_{geo}(\theta)$ is the probability for a water molecule to be on the liquid−gas surface, which is a geometry-related factor. From the microscopic point of view, an evaporation event is a process where a water molecule on the outermost layer of the condensed water gains enough kinetic energy over the energy barrier to evaporate and fly into the vacuum. The probability for the water molecules on this outermost region varies with the shape of the water droplet, which can be denoted as a function of the contact angle $\theta$ of the water droplet. $P_{ener}(E)$ is the escape probability of a surficial water molecule. We find that the variation of the evaporation flux is the result of a combination of the geometric and the energetic factors.

**$N_{surf}/N_{cond}$ Ratio.** With respect to molecular dynamics simulation, $P_{geo}(\theta)$ is defined as the ratio of the number of surficial water molecules $N_{surf}$, to the total number of all condensed water molecules $N_{cond}$

$$P_{geo}(\theta) = \frac{N_{surf}(\theta)}{N_{cond}} \quad (2)$$

The theoretical derivation of $P_{geo}(\theta)$ is in the Supporting Information. In Figure 4a, we show the evaporation flux of different contact angles $\theta$. The black curve with the error bars is the evaporation flux calculated from the MD trajectory, and the red curve is a simulated curve of $P_{geo}(\theta)$ to fit the MD data. We can learn from Figure 4a that $P_{geo}(\theta)$ can fit the black curve when $\theta$ is larger than 20°, which is within the region of $q < 0.4$ e. On the other hand, the $N_{surf}$ and $N_{cond}$ can also be calculated directly from the MD trajectory. Figure 4b shows the $N_{surf}/N_{cond}$ ratio on the basis of the MD trajectory. From Figure 4b, we can see that the variation of the $N_{surf}/N_{cond}$ ratio can also fit the $J(q)$ curve when $q < 0.4$ e. Hence, we can conclude that, when $q < 0.4$ e, the variation of the evaporation flux $J(q)$ is mainly affected by the variation of the water−gas interface area


dx.doi.org/10.1021/jp302142s | J. Phys. Chem. B 2012, 116, 13863−13867

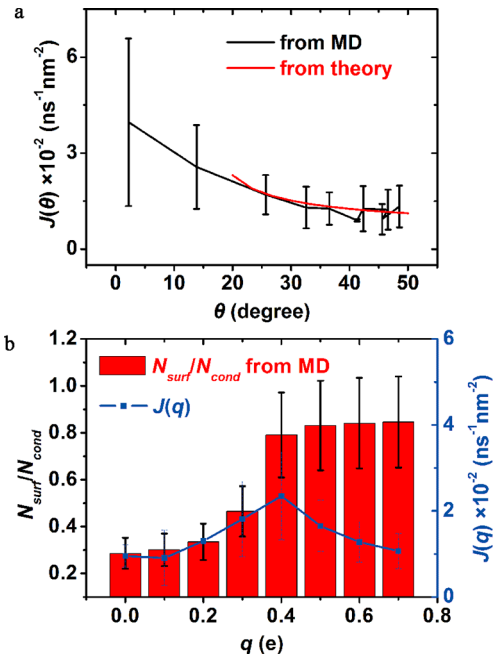


**Figure 4.** (a) The evaporation flux versus contact angle $\theta$. The black line with error bars is calculated from MD, and the red line is the theoretical fit. (b) The $N_{surf}/N_{cond}$ ratio versus $q$ calculated from the nonequilibrium MD trajectory (red columns) together with the evaporation flux $J(q)$.

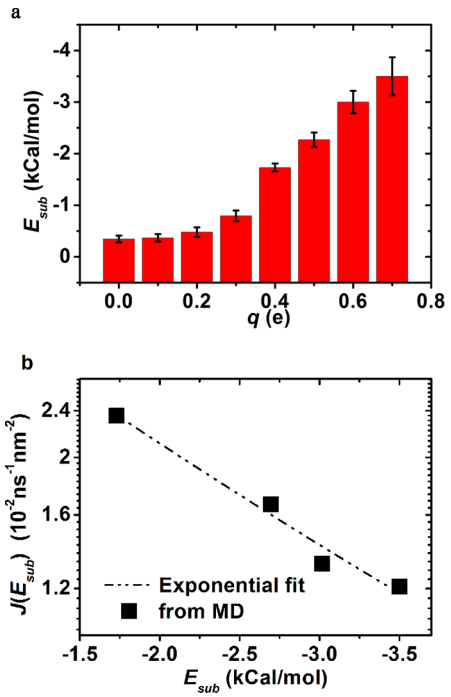


**Figure 5.** (a) The attraction energy to the outermost layer water molecules provided by the ionic substrate solid surface ($E_{sub}$) versus the assigned charge $q$. (b) The MD evaporation flux (black square points) and its exponential fit with respect to $E_{sub}$ (black dashed line) in a semilog plot.

of the condensed water: when $q$ is enhanced, the water aggregation becomes flatter (the contact angle $\theta$ becomes smaller) and the surface area of the condensed water increases, which cause the increase of the evaporation speed.

**Evaporation Barrier $E_{sub}$.** When discussing the evaporation event, we are interested in the water molecules that are in the outermost layer of the adsorbed water aggregation because they are the candidates for leaving the restriction of the ionic solid surface. Besides their number, the attraction potential barrier that keeps them from escaping the solid surface is also an important factor that influences the evaporation speed of the adsorbed water aggregation. When $q \geq 0.4$ e, the adhered water forms a flat single-layer molecular sheet with only a few overlapping water molecules, and the contact angle $\theta$ does not change with $q$. Therefore, formula 1 can be written as

$$J(q) \propto P_{ener}(E_{sub}(q)) \quad (3)$$

$E_{sub}$ is the interaction energy from the substrate, mainly provided by the electrical charge $q$ assigned on the substrate. Note that $E_{sub}$ is different from $E_s$ in Figure 2b: the object of $E_{sub}$ is the outermost layer water molecules, but the object of $E_s$ is the water molecules in the first hydration layer, which is within 3 Å of the solid surface. We plot the $E_{sub}(q)$ profile in Figure 5a. From Figure 5a, we learn that the magnitude of $E_{sub}$ increase with the enhancing of the surface charge $q$. Comparing with the increment of $E_{sub}$ for $q \geq 0.4$ e, the increments of $E_{sub}$ for $q < 0.4$ e are negligible. For $q \geq 0.4$ e, $E_{sub}$ increases proportionally with $q$, and the increment of $E_{sub}$ is about 0.5kcal/mol as $q$ increases every 0.1 e.

The speed distribution of the water molecules in this work satisfies the Maxwell distribution because the Berendsen thermostat was employed in this work. According to the thermodynamics, for the system under the NVT ensemble, the probability for a free molecule to gain kinetic energy more than the energy barrier $E_0$ is proportional to $\exp(-(E_0/k_BT))$.[53,58] In our simulation, when $q \geq 0.4$ e, the evaporation flux decreases almost exponentially with respect to $E_{sub}$, as shown in Figure 5b The exponential decreasing of the evaporation flux with the enhancing of $E_{sub}$ indicates that, when the water spreads smoothly across the substrate, the attraction from the substrate becomes the main factor that impacts the water evaporation.

## CONCLUSION

The effect of the surface wettability of the substrate on the evaporation of the nanoscale water aggregation adhered on it is the competition of two different mechanisms: one is the surface wettability influencing the shape of the liquid−gas surface of the water aggregation; the other is the attraction provided by the substrate of different wettabilities changing the escape probability of surficial water molecules. When the surface wettability of the substrate is not high enough, the water molecules accumulate into the form of a sessile spherical cap. The predominant factor that affects the evaporation flux is the geometrical shape of the water aggregation. The surface area of the droplet is the main factor that influences the evaporation flux. Since the surface area of the droplet increases as the contact angle decreases, the evaporation flux increases as the surface wettability increases. Meanwhile, when the surface wettability of the substrate is high enough, the water molecules spread to a monolayer and the geometric factor no longer affects much because the form of the water aggregation almost remains the same. In this situation, when the surface wettability increases, the energy barrier provided by the substrate that prevents the water molecules from running off becomes stronger, which causes the decreasing of the evaporation flux.

This study of the effect of the surface wettability on the evaporation of a nanoscale water aggregation may enlighten the


dx.doi.org/10.1021/jp302142s | J. Phys. Chem. B 2012, 116, 13863−13867

study of multiple natural evaporation processes that are related to the ultrathin water aggregation, which is very important for biological and environmental science.

## ■ ASSOCIATED CONTENT

### Supporting Information

The derivation of the geometric factor that dominantly regulates the evaporating speed when surface charge $q < 0.4$ e is included in the Supporting Information. This material is available free of charge via the Internet at http://pubs.acs.org.

## ■ AUTHOR INFORMATION

### Corresponding Author

*E-mail: wanrongzheng@sinap.ac.cn.

### Notes

The authors declare no competing financial interest.

## ■ ACKNOWLEDGMENTS

We gratefully acknowledge Profs. Xinguang Zhu and Yi Gao and Drs. Chunlei Wang and Wenpeng Qi for their helpful discussions. This work was supported by NNSFC (10825520, 11105088), SLADP (B111), IPSHMEC (11YZ20), the Knowledge Innovation Program of the Chinese Academy of Sciences, and Shanghai Supercomputer Center of China.

## ■ REFERENCES

(1) Penman, H. L. *Proc. R. Soc. London, Ser. A* **1948**, *193*, 120−145.
(2) Kohler, M. A.; Parmele, L. H. *Water Resour. Res.* **1967**, *3*, 997−1005.
(3) Eames, I. W.; Marr, N. J.; Sabir, H. *Int. J. Heat Mass Transfer* **1997**, *40*, 2963−2973.
(4) Ramanathan, V.; Crutzen, P. J.; Kiehl, J. T.; Rosenfeld, D. *Science* **2001**, *294*, 2119−2124.
(5) Lopez Cascales, J. J.; Berendsen, H. J. C.; Garcia de la Torre, J. *J. Phys. Chem.* **1996**, *100*, 8621−8627.
(6) Miranda, P. B.; Xu, L.; Shen, Y. R.; Salmeron, M. *Phys. Rev. Lett.* **1998**, *81*, 5876.
(7) James, M.; Darwish, T. A.; Ciampi, S.; Sylvester, S. O.; Zhang, Z.; Ng, A.; Gooding, J. J.; Hanley, T. L. *Soft Matter* **2011**, *7*, 5309−5318.
(8) Godawat, R.; Jamadagni, S. N.; Garde, S. *Proc. Natl. Acad. Sci. U.S.A.* **2009**, *106*, 15119−15124.
(9) Kimmel, G. A.; Petrik, N. G.; Dohnálek, Z.; Kay, B. D. *Phys. Rev. Lett.* **2005**, *95*, 166102.
(10) Xu, D.; Liechti, K. M.; Ravi-Chandar, K. *Langmuir* **2009**, *25*, 12870−12873.
(11) Janecek, J.; Netz, R. R. *Langmuir* **2007**, *23*, 8417−8429.
(12) Sendner, C.; Horinek, D.; Bocquet, L.; Netz, R. R. *Langmuir* **2009**, *25*, 10768−10781.
(13) Russell, J. T.; Wang, B.; Král, P. *J. Phys. Chem. Lett.* **2012**, *3*, 353−357.
(14) Vuković, L.; Král, P. *Phys. Rev. Lett.* **2009**, *103*, 246103.
(15) Wang, Y.; Zhao, Y. J.; Huang, J. P. *J. Phys. Chem. B* **2011**, *115*, 13275−13279.
(16) Sharp, K. A.; Vanderkooi, J. M. *Acc. Chem. Res.* **2010**, *43*, 231−239.
(17) Stevens, M. J.; Grest, G. S. *Biointerphases* **2008**, *3*, FC13−FC22.
(18) Wang, C.; Zhou, B.; Tu, Y.; Duan, M.; Xiu, P.; Li, J.; Fang, H. *Sci. Rep.* **2012**, *2*, 358.
(19) Wang, C.; Zhou, B.; Xiu, P.; Fang, H. *J. Phys. Chem. C* **2011**, *115*, 3018−3024.
(20) Das, P.; Zhou, R. *J. Phys. Chem. B* **2010**, *114*, 5427−5430.
(21) Tsai, P.; Lammertink, R. G. H.; Wessling, M.; Lohse, D. *Phys. Rev. Lett.* **2009**, *104*, 116102.
(22) Gordillo, M. C.; Marti, J. *J. Chem. Phys.* **2002**, *117*, 3425−3430.
(23) Xiu, P.; Yang, Z.; Zhou, B.; Das, P.; Fang, H.; Zhou, R. *J. Phys. Chem. B* **2011**, *115*, 2988−2994.
(24) Zarei, G.; Homaee, M.; Liaghat, A. M.; Hoorfar, A. H. *J. Hydrol. (Amsterdam, Neth.)* **2010**, *380*, 356−361.
(25) Nag, K.; Perez-Gil, J.; Ruano, M. L. F.; Worthman, L. A. D.; Stewart, J.; Casals, C.; Keough, K. M. W. *Biophys. J.* **1998**, *74*, 2983−2995.
(26) Sefiane, K. *J. Colloid Interface Sci.* **2004**, *272*, 411−419.
(27) Ghosh, A.; Campen, R. K.; Sovago, M.; Bonn, M. *Faraday Discuss.* **2009**, *141*, 145−159.
(28) Kauzmann, W. *Adv. Protein Chem.* **1959**, *14*, 1−63.
(29) Liu, P.; Huang, X.; Zhou, R.; Berne, B. J. *Nature* **2005**, *437*, 159−162.
(30) Hua, L.; Huang, X.; Liu, P.; Zhou, R.; Berne, B. J. *J. Phys. Chem. B* **2007**, *111*, 9069−9077.
(31) Das, P.; Matysiak, S.; Clementi, C. *Proc. Natl. Acad. Sci. U.S.A.* **2005**, *102*, 10141−10146.
(32) Koga, K.; Tanaka, H.; Zeng, X. C. *Nature* **2000**, *408*, 564−567.
(33) Lee, M.; Lee, D.; Jung, N.; Yun, M.; Yim, C.; Jeon, S. *Appl. Phys. Lett.* **2011**, *98*, 013107−013103.
(34) Gu, W.; Zhou, B.; Geyer, T.; Hutter, M.; Fang, H.; Helms, V. *Angew. Chem., Int. Ed* **2011**, *123*, 794−797.
(35) Gu, W.; Zhou, B.; Geyer, T.; Hutter, M.; Fang, H.; Helms, V. *Angew. Chem., Int. Ed.* **2011**, *50*, 768−771.
(36) Wan, R. Z.; Li, J. Y.; Lu, H. J.; Fang, H. P. *J. Am. Chem. Soc.* **2005**, *127*, 7166−7170.
(37) Wang, C.; Lu, H.; Wang, Z.; Xiu, P.; Zhou, B.; Zuo, G.; Wan, R.; Hu, J.; Fang, H. *Phys. Rev. Lett.* **2009**, *103*, 137801.
(38) Chan, H.; Kral, P. *Nanoscale* **2011**, *3*, 1181−1186.
(39) Schwierz, N.; Horinek, D.; Netz, R. R. *Langmuir* **2010**, *26*, 7370−7379.
(40) Talapin, D. V.; Shevchenko, E. V.; Murray, C. B.; Titov, A. V.; Král, P. *Nano Lett.* **2007**, *7*, 1213−1219.
(41) Titov, A. V.; Kral, P. *Nano Lett.* **2008**, *8*, 3605−3612.
(42) Moussa, S. G.; McIntire, T. M.; Szöri, M.; Roeselová, M.; Tobias, D. J.; Grimm, R. L.; Hemminger, J. C.; Finlayson-Pitts, B. J. *J. Phys. Chem. A* **2009**, *113*, 2060−2069.
(43) Zhakhovskii, V.; Anisimov, S. *J. Exp. Theor. Phys.* **1997**, *84*, 734−745.
(44) Jorgensen, W. L.; Chandrasekhar, J.; Madura, J. D.; Impey, R. W.; Klein, M. L. *J. Chem. Phys.* **1983**, *79*, 926−935.
(45) Lu, D.; Li, Y.; Ravaioli, U.; Schulten, K. *J. Phys. Chem. B* **2005**, *109*, 11461−11467.
(46) Goldsmith, J.; Martens, C. C. *J. Phys. Chem. Lett.* **2009**, *1*, 528−535.
(47) Phillips, J. C.; Braun, R.; Wang, W.; Gumbart, J.; Tajkhorshid, E.; Villa, E.; Chipot, C.; Skeel, R. D.; Kalé, L.; Schulten, K. *J. Comput. Chem.* **2005**, *26*, 1781−1802.
(48) Berendsen, H. J. C.; Postma, J. P. M.; van Gunsteren, W. F.; DiNola, A.; Haak, J. R. *J. Chem. Phys.* **1984**, *81*, 3684−3690.
(49) Gelderblom, H.; Marin, A. G.; Nair, H.; van Houselt, A.; Lefferts, L.; Snoeijer, J. H.; Lohse, D. *Phys. Rev. E: Stat. Phys., Plasmas, Fluids, Relat. Interdiscip. Top* **2011**, *83*, 026306.
(50) Szöri, M.; Jedlovszky, P.; Roeselova, M. *Phys. Chem. Chem. Phys.* **2010**, *12*, 4604−4616.
(51) Szöri, M.; Tobias, D. J.; Roeselová, M. *J. Phys. Chem. B* **2009**, *113*, 4161−4169.
(52) Guo, H.-K.; Fang, H.-P. *Chin. Phys. Lett.* **2005**, *22*, 787.
(53) Ward, C. A.; Fang, G. *Phys. Rev. E: Stat. Phys., Plasmas, Fluids, Relat. Interdiscip. Top* **1999**, *59*, 429.
(54) Tsuruta, T.; Nagayama, G. *J. Phys. Chem. B* **2004**, *108*, 1736−1743.
(55) Meland, R.; Frezzotti, A.; Ytrehus, T.; Hafskjold, B. *Phys. Fluids* **2004**, *16*, 223−243.
(56) Yi, P.; Poulikakos, D.; Walther, J.; Yadigaroglu, G. *Int. J. Heat Mass Transfer* **2002**, *45*, 2087−2100.
(57) Tsuruta, T.; Tanaka, H.; Masuoka, T. *Int. J. Heat Mass Transfer* **1999**, *42*, 4107−4116.
(58) Bond, M.; Struchtrup, H. *Phys. Rev. E: Stat. Phys., Plasmas, Fluids, Relat. Interdiscip. Top* **2004**, *70*, 061605.